EUROPEAN ORGANIZATION FOR NUCLEAR RESEARCH

CERN-PH-EP/2005-021
May 12, 2005

Measurement of the Running of the Electromagnetic Coupling at Large Momentum-Transfer at LEP

The L3 Collaboration

Abstract

The evolution of the electromagnetic coupling, α, in the momentum-transfer range $1800\ \mathrm{GeV}^2 < -Q^2 < 21600\ \mathrm{GeV}^2$ is studied with about 40 000 Bhabha-scattering events collected with the L3 detector at LEP at centre-of-mass energies $\sqrt{s} = 189 - 209$ GeV. The running of α is parametrised as:

$$\alpha(Q^2) = \frac{\alpha_0}{1 - C\Delta\alpha(Q^2)},$$

where $\alpha_0 \equiv \alpha(Q^2 = 0)$ is the fine-structure constant and $C = 1$ corresponds to the evolution expected in QED. A fit to the differential cross section of the $e^+e^- \to e^+e^-$ process for scattering angles in the range $|\cos\theta| < 0.9$ excludes the hypothesis of a constant value of α, $C = 0$, and validates the QED prediction with the result:

$$C = 1.05 \pm 0.07 \pm 0.14,$$

where the first uncertainty is statistical and the second systematic.

Submitted to *Phys. Lett. B*

1 Introduction

A fundamental consequence of quantum field theory is that the value of the electromagnetic coupling, α, depends on, or *runs* with, the squared momentum transfer, Q^2. This phenomenon is due to higher momentum-transfers probing virtual-loop corrections to the photon propagator. This process of *vacuum polarisation* is sketched in Figure 1. In QED, the dependence of α on Q^2 is described as [2]:

$$\alpha(Q^2) = \frac{\alpha_0}{1 - \Delta\alpha(Q^2)}, \tag{1}$$

where the fine-structure constant, $\alpha_0 \equiv \alpha(Q^2 = 0)$, is a fundamental quantity of Physics. It is measured with high accuracy in solid-state processes and via the study of the anomalous magnetic moment of the electron to be $1/\alpha_0 = 137.03599911 \pm 0.00000046$ [1]. The contributions to $\Delta\alpha(Q^2)$ from lepton loops are precisely predicted [3], while those from quark loops are difficult to calculate due to non-perturbative QCD effects. They are estimated using dispersion-integral techniques [4] and information from the $e^+e^- \to$ *hadrons* cross section. At the scale of the Z-boson mass, recent calculations yield $\alpha^{-1}(m_Z^2) = 128.936 \pm 0.046$ [5]. Similar results, with smaller uncertainty, are found by other evaluations using stronger theoretical assumptions. For example, Reference 6 obtains $\alpha^{-1}(m_Z^2) = 128.962 \pm 0.016$.

The running of α was studied at e^+e^- colliders both in the *time-like* region, $Q^2 > 0$, and the *space-like* region, $Q^2 < 0$. The first measurement in the time-like region was performed by the TOPAZ Collaboration at TRISTAN for $Q^2 = 3338$ GeV^2 by comparing the cross sections of the $e^+e^- \to e^+e^-$ and $e^+e^- \to e^+e^-\mu^+\mu^-$ processes [7]. The OPAL Collaboration at LEP exploited the different sensitivity to $\alpha(Q^2)$ of the cross sections of the $e^+e^- \to \mu^+\mu^-$, $e^+e^- \to \tau^+\tau^-$ and $e^+e^- \to q\bar{q}$ processes above the Z resonance to determine $\alpha(37236\ \text{GeV}^2)$ [8]. Information on $\alpha(m_Z^2)$ is also extracted from the couplings of the Z boson to fermion pairs [9].

Bhabha scattering at e^+e^- colliders, $e^+e^- \to e^+e^-$, gives access to the running of α in the space-like region. In addition, like other processes dominated by t-channel photon exchange, it has little dependence on weak corrections. The four-momentum transfer in Bhabha scattering depends on s and on the scattering angle, θ: $Q^2 = t \simeq -s(1 - \cos\theta)/2 < 0$. Small-angle and large-angle Bhabha scattering allow to probe the running of α in different Q^2 ranges.

LEP detectors were equipped with luminosity monitors, high-precision calorimeters located close to the beam pipe and designed to measure small-angle Bhabha scattering in order to determine the integrated luminosity collected by the experiments. The L3 collaboration first established the running of α in the range $2.10\ \text{GeV}^2 < -Q^2 < 6.25\ \text{GeV}^2$ [10] by comparing event counts in different regions of its luminosity monitor. More recently, the OPAL Collaboration studied the similar range $1.81\ \text{GeV}^2 < -Q^2 < 6.07\ \text{GeV}^2$ [11].

The running of α in large-angle Bhabha scattering was first investigated by the VENUS Collaboration at TRISTAN in the range $100\ \text{GeV}^2 < -Q^2 < 2916\ \text{GeV}^2$ [12]. Later, the L3 Collaboration studied the same process at $\sqrt{s} = 189$ GeV for scattering angles $0.81 < |\cos\theta| < 0.94$, probing the range $12.25\ \text{GeV}^2 < -Q^2 < 3434\ \text{GeV}^2$ [10].

This Letter investigates the running of α by studying the differential cross section for Bhabha scattering at LEP at $\sqrt{s} = 189 - 209$ GeV for scattering angles such that $|\cos\theta| < 0.9$. Less than 1% of the events scatter backwards, $\cos\theta < 0$, and this analysis effectively probes the region $1800\ \text{GeV}^2 < -Q^2 < 21600\ \text{GeV}^2$, extending and complementing previous space-like studies.

2 Analysis Strategy

In the following, the running of α is described by a free parameter, C, defined according to:

$$\alpha(Q^2) = \frac{\alpha_0}{1 - C\Delta\alpha(Q^2)}, \tag{2}$$

where the parametrisation of Reference 5 is used for the term $\Delta\alpha(Q^2)$. A value of C consistent with $C = 1$ would indicate that data follow the behaviour predicted by QED, while the hypothesis $\alpha = \alpha_0$, with no dependence on Q^2, corresponds to $C = 0$.

The value of C is derived by a study of the measured differential cross section of the $e^+e^- \to e^+e^-$ process, $d\sigma/d\cos\theta$. This quantity depends on C through the measured integrated luminosity, $\mathcal{L}(C)$, which is calculated from the expected cross section of the $e^+e^- \to e^+e^-$ process for small scattering angles. The measurements used in the following are obtained under the Standard Model hypothesis, $C = 1$, as:

$$\frac{d\sigma(1)}{d\cos\theta} = \frac{N(\cos\theta)}{\Delta\cos\theta}\frac{1}{\mathcal{L}(1)\varepsilon(\cos\theta)}, \tag{3}$$

where $N(\cos\theta)$ is the number of events observed in a given $\cos\theta$ range, of width $\Delta\cos\theta$, with average acceptance $\varepsilon(\cos\theta)$. The measured integrated luminosity depends on C as:

$$\mathcal{L}(C) \equiv \frac{N_L}{\sigma_L(C)\varepsilon_L(C)} = \mathcal{L}(1)\frac{\sigma_L(1)\varepsilon_L(1)}{\sigma_L(C)\varepsilon_L(C)}, \tag{4}$$

where N_L is the number of events observed in the fiducial volume of the luminosity monitor, $\sigma_L(C)$ is the corresponding $e^+e^- \to e^+e^-$ cross section for a given value of C and $\varepsilon_L(C)$ is the detector acceptance. This acceptance may depend on C due to the combined effect of small angular anisotropies of detector efficiencies and the dependence of the predicted differential cross section on C. These changes in the acceptance are found to have negligible impact on the results presented below.

The value of the parameter C is extracted by comparing the measured differential cross section to the theoretical prediction as a function of C, $d\sigma^{th}(C)/d\cos\theta$, derived as:

$$\frac{d\sigma^{th}(C)}{d\cos\theta} \equiv \frac{d\sigma^{th}(1)}{d\cos\theta}\frac{\mathcal{L}(1)}{\mathcal{L}(C)}, \tag{5}$$

where $d\sigma^{th}(1)/d\cos\theta$ is the Standard Model prediction, discussed in Reference 13. The value of $\mathcal{L}(1)$ is derived by using the BHLUMI Monte Carlo program [14]. The dependence of $d\sigma^{th}(C)/d\cos\theta$ and $\mathcal{L}(C)$ on C is implemented by means of the BHWIDE Monte Carlo program [15]. The differential cross section is factorised as:

$$\frac{d\sigma^{th}(C)}{d\cos\theta} \equiv \frac{d\sigma^{Born}(C)}{d\cos\theta}F_{rad}\left(\cos\theta\right), \tag{6}$$

where $d\sigma^{Born}(C)/d\cos\theta$ is the tree-level differential cross section, which has a simple analytical form. The term $F_{rad}\left(\cos\theta\right)$ parametrises initial-state and final-state radiation effects, dominated by real-photon emission, as implemented in BHWIDE. It is verified that $F_{rad}\left(\cos\theta\right)$ has a negligible dependence on the spread of $\sqrt{s}$ considered in this analysis and, most important, on C.

3 Cross Section Measurement

The data were collected at LEP by the L3 detector [16,17] in the years from 1998 through 2000. They correspond to an integrated luminosity of 607.4 pb^{-1} and are grouped in eight intervals of $\sqrt{s}$ with the average values and corresponding integrated luminosities listed in Table 1.

Events from the $\mathrm{e^+e^-} \to \mathrm{e^+e^-}$ process are selected as described in Reference 18. Electrons and positrons are identified as clusters in the BGO electromagnetic calorimeter, matched with tracks in the central tracker. In the barrel region of the detector, $|\cos\theta| < 0.72$, the energy of the most energetic cluster must satisfy $E_1 > 0.25\sqrt{s}$, while the energy of the other cluster must satisfy $E_2 > 20$ GeV. In the endcap region, $0.81 < |\cos\theta| < 0.98$, these criteria are relaxed to $E_1 > 0.2\sqrt{s}$ and $E_2 > 10$ GeV. Events with clusters in the transition region between the barrel and endcap regions, $0.72 < |\cos\theta| < 0.81$, instrumented with a lead and scintillating-fiber calorimeter [17], are rejected. To suppress contributions from events with high-energy initial-state radiation, the complement to 180° of the angle between the two clusters, the acollinearity, ζ, is required to be less than 25°. The number of events observed at different values of $\sqrt{s}$ is shown in Table 1 together with the Monte Carlo expectations for signal and background.

The $\mathrm{e^+e^-} \to \mathrm{e^+e^-}$ process is simulated with the BHWIDE Monte Carlo generator assuming $C = 1$. Background processes are described with the following Monte Carlo generators: KORALZ [19] for $\mathrm{e^+e^-} \to \tau^+\tau^-$, KORALW [20] for $\mathrm{e^+e^-} \to \mathrm{W^+W^-}$, PYTHIA [21] for $\mathrm{e^+e^-} \to \mathrm{Ze^+e^-}$, DIAG36 [22] for $\mathrm{e^+e^-} \to \mathrm{e^+e^-e^+e^-}$, GGG [23] for $\mathrm{e^+e^-} \to \gamma\gamma\gamma$ and TEEGG [24] for $\mathrm{e^+e^-} \to \mathrm{e^+e^-}\gamma$ events where one fermion is scattered into the beam pipe and the photon is in the detector. The L3 detector response is simulated using the GEANT package [25], which describes effects of energy loss, multiple scattering and showering in the detector. Time-dependent detector inefficiencies, as monitored during the data-taking period, are included in the simulation.

Systematic effects, such as charge confusion, are reduced by folding the differential cross section into $\mathrm{d}\sigma/\mathrm{d}|\cos\theta|$, which is defined as:

$$\frac{\mathrm{d}\sigma}{\mathrm{d}|\cos\theta|} \equiv \frac{\mathrm{d}\sigma}{\mathrm{d}\cos\theta}\Big|_{\cos\theta<0} + \frac{\mathrm{d}\sigma}{\mathrm{d}\cos\theta}\Big|_{\cos\theta>0}. \tag{7}$$

This differential cross section is measured in the fiducial volume defined by:

$$12^\circ < \theta_{\mathrm{e^-,e^+}} < 168^\circ \tag{8}$$

$$|\cos\theta| < 0.9 \tag{9}$$

$$\zeta < 25^\circ \tag{10}$$

where $\theta_{\mathrm{e^-}}$ and $\theta_{\mathrm{e^+}}$ are the polar angles of the electron and the positron, respectively. The value of $\cos\theta$ is derived as:

$$\cos\theta \equiv \frac{\sin|\theta_{\mathrm{e^+}} - \theta_{\mathrm{e^-}}|}{\sin\theta_{\mathrm{e^-}} + \sin\theta_{\mathrm{e^+}}}. \tag{11}$$

Ten intervals of $|\cos\theta|$ are considered for each of the eight values of $\sqrt{s}$, for a total of 80 independent measurements. Table 2 and Figure 2 present the measurements of $\mathrm{d}\sigma/\mathrm{d}|\cos\theta|$ and the Standard Model expectations. The larger uncertainties in the interval $0.72 - 0.81$ are due to the transition region between the barrel and the endcap regions.

4 Results

Figures 3 and 4 compare the combined differential cross section at the average centre-of-mass energy $\langle\sqrt{s}\rangle = 198$ GeV with the Standard Model prediction, corresponding to $C = 1$, and with a constant value of α, corresponding to $C = 0$. The data favour the hypothesis $C = 1$ over the hypothesis $C = 0$, as also presented in Table 3.

The value of C is extracted by comparing the 80 measurements of $\mathrm{d}\sigma/\mathrm{d}|\cos\theta|$ with the theoretical expectations $\mathrm{d}\sigma^{th}(C)/\mathrm{d}\cos\theta$ in a χ^2 fit with the result:

$$C = 1.06 \pm 0.07,$$

where the quoted uncertainty is statistical only. Several sources of systematic uncertainties are then considered.

- The theoretical expectations for $\mathrm{d}\sigma^{th}(1)/\mathrm{d}\cos\theta$ have an uncertainty which varies from 0.5% in the endcap region to 1.5% in the barrel region [13, 15].
- The measurements of $\mathrm{d}\sigma/\mathrm{d}|\cos\theta|$ are affected by a systematic uncertainty, dominated by the event-selection procedure, which varies between 1% and 10%, as listed in Table 2 [18].
- An uncertainty between 0.2% and 1.5% is assigned to $F_{rad}\,(\cos\theta)$, as a function of $\cos\theta$, in order to account for possible higher-order effects not included in the BHWIDE parametrisation.
- Migration effects among the different $\cos\theta$ bins are found to be negligible due to the large bin size and the good detector resolution.

Systematic uncertainties are conservatively treated as fully correlated and the fit is repeated including both statistical and systematic uncertainties with the result:

$$C = 1.05 \pm 0.07 \pm 0.14,$$

where the first uncertainty is statistical and the second systematic. A breakdown of the systematic uncertainty is presented in Table 4. This result is in agreement with the Standard Model expectation, $C = 1$. The quality of the fit is satisfactory, with a χ^2 of 91.9 for 79 degrees of freedom, corresponding to a confidence level of 17%. The hypothesis of a value of α which does not depend on Q^2, $C = 0$, is totally excluded with a χ^2 of 316 for 80 degrees of freedom, corresponding to a a confidence level of 10^{-29}.

5 Discussion

The result presented above establishes the evolution of the electromagnetic coupling with $-Q^2$ in the range $1800\ \mathrm{GeV}^2 < -Q^2 < 21600\ \mathrm{GeV}^2$. This finding extends and complements studies based on small-angle Bhabha scattering by the L3 [10] and OPAL [11] Collaborations, which studied the regions $2.10\ \mathrm{GeV}^2 < -Q^2 < 6.25\ \mathrm{GeV}^2$ and $1.81\ \mathrm{GeV}^2 < -Q^2 < 6.07\ \mathrm{GeV}^2$, respectively. The advantage of large-angle Bhabha scattering, investigated in this Letter, is to probe large values of $-Q^2$, while studies of small-angle Bhabha scattering at lower values of $-Q^2$ benefit from a larger cross section and thus statistical accuracy. The experimental systematic uncertainties of measurements in the two $-Q^2$ regions are implicitly different. At large $-Q^2$, they are dominated by the selection of Bhabha events in the large-angle calorimeters, while at

low $-Q^2$ they mostly arise from the event reconstruction in the luminosity monitors and from effects of the material traversed by electrons and positrons before their detection. Both studies, at large and low $-Q^2$, are affected by theoretical uncertainties on the differential cross section of Bhabha scattering, although in different angular regions

Figures 5 and 6 present the evolution of the electromagnetic coupling with $-Q^2$. A band for 1800 GeV^2 $< -Q^2 <$ 21600 GeV^2 shows the 68% confidence level result from this analysis. It is derived by inserting the measured value of C with its errors in Equation (2) together with the QED predictions of Reference 5. The results from previous L3 data for Bhabha scattering at 2.10 GeV^2 $< -Q^2 <$ 6.25 GeV^2 and 12.25 GeV^2 $< -Q^2 <$ 3434 GeV^2 [10] are also shown. These two measurements are not absolute measurements of the electromagnetic coupling but differences between the values of $\alpha(Q^2)$ at the extreme of the Q^2 ranges [10]:

$$\alpha^{-1}(-2.10\ \text{GeV}^2) - \alpha^{-1}(-6.25\ \text{GeV}^2) = 0.78 \pm 0.26 \quad (12)$$

$$\alpha^{-1}(-12.25\ \text{GeV}^2) - \alpha^{-1}(-3434\ \text{GeV}^2) = 3.80 \pm 1.29. \quad (13)$$

The results in Figure 5 are obtained by fixing the values of $\alpha(-2.10\ \text{GeV}^2)$ and $\alpha(-12.25\ \text{GeV}^2)$ to the QED predictions of Reference 5 in order to extract the values of $\alpha(-6.25\ \text{GeV}^2)$ and $\alpha(-3434\ \text{GeV}^2)$ from Equations (12) and (13). The results shown in Figure 6 are obtained by first determining the values of $\alpha(-2.10\ \text{GeV}^2)$ and $\alpha(-12.25\ \text{GeV}^2)$ from the measured value of C and from Equation (2) and then extracting the values of $\alpha(-6.25\ \text{GeV}^2)$ and $\alpha(-3434\ \text{GeV}^2)$ from Equations (12) and (13). This procedure relies on the assumption that the measured value of C also describes the running of the electromagnetic coupling for lower values of $-Q^2$. Both figures provide an impressive evidence of the running of the electromagnetic coupling in the energy range accessible at LEP.

References

[1] CODATA Task Group, Rev. Mod. Phys. **72** (2000) 351;
`http://physics.nist.gov/constants`.

[2] E.C.G. Stückelberg and A. Petermann, Helv. Phys. Acta **26** (1953) 499;
M. Gell-Mann and F. Low, Phys. Rev. **95** (1954) 1300;
N.N. Bogoliubov and D.V. Shirkov, Dokl. AN SSSR **103** (1955) 203.

[3] M. Steinhauser, Phys. Lett. **B 429** (1998) 158.

[4] N. Cabibbo and R. Gatto, Phys. Rev. **124** (1961) 1577.

[5] H. Burkhardt and B. Pietrzyk, Phys. Lett. **B 513** (2001) 46.

[6] J.F. Trocóniz and F.J. Ynduráin, Phys. Rev. **D 71** (2005) 073008.

[7] TOPAZ Collab., I. Levine *et al.*, Phys. Rev. Lett. **78** (1997) 424.

[8] OPAL Collab., G. Abbiendi *et al.*, Eur. Phys. J. **C 33** (2004) 173.

[9] S. Banerjee and S.N. Ganguli, Z. Phys. **C 57** (1993) 229;
D. Abbaneo *et al.*, *A combination of preliminary electroweak measurements and constraints on the Standard Model*, preprint hep-ex/0412015 (2004).

[10] L3 Collab., M. Acciarri *et al.*, Phys. Lett. **B 476** (2000) 40.

[11] OPAL Collab. G. Abbiendi *et al.*, *Measurement of the running of the QED coupling in small-angle Bhabha scattering at LEP*, preprint CERN-PH-EP-2005-014 (2005).

[12] VENUS Collab., S. Odaka *et al.*, Phys. Rev. Lett. **81** (1998) 2428; VENUS Collab., T. Arima *et al.*, Phys. Rev. **D 55** (1997) 19.

[13] M. Kobel *et al.*, *Two-fermion production in electron positron collisions*, CERN Report 2000-009, 2000, p. 292, hep-ph/0007180; and references therein.

[14] BHLUMI version 4.04 is used;
S. Jadach *et al.*, Comp. Phys. Comm. **102** (1997) 229.

[15] BHWIDE version 1.03 is used;
S. Jadach, W. Placzek and B.F.L. Ward, Phys. Lett. **B 390** (1997) 298.

[16] L3 Collab., B. Adeva *et al.*, Nucl. Inst. Meth. **A 289** (1990) 35;
L3 Collab., O. Adriani *et al.*, Physics Reports **236** (1993) 1;
M. Acciarri *et al.*, Nucl. Inst. Meth. **A 351** (1994) 300;
M. Chemarin *et al.*, Nucl. Inst. Meth. **A 349** (1994) 345;
A. Adam *et al.*, Nucl. Inst. Meth. **A 383** (1996) 342;
I.C. Brock *et al.*, Nucl. Inst. Meth. **A 381** (1996) 236.

[17] G. Basti *et al.*, Nucl. Inst. Meth. **A 374** (1996) 293.

[18] L3 Collab., M. Acciarri *et al.*, Phys. Lett. **B 479** (2000) 101;
L3 Collab., P. Achard *et al.*, *Measurement of Hadron and Lepton Pair Production at* 192 GeV $< \sqrt{s} <$ 209 GeV *at LEP*, in preparation;
Patrick Déglon, *Étude de la diffusion Bhabha avec le détecteur L3 au LEP*, Ph.D. thesis, University of Geneva, 2002.

[19] KORALZ version 4.04 is used;
S. Jadach *et al.*, Comp. Phys. Comm. **79** (1994) 503.

[20] KORALW version 1.513 is used;
S. Jadach *et al.*, Comp. Phys. Comm. **119** (1999) 272.

[21] PYTHIA versions 5.722 is used;
T. Sjöstrand, preprint CERN-TH/7112/93 (1993), revised 1995;
T. Sjöstrand, Comp. Phys. Comm. **82** (1994) 74.

[22] DIAG36 version 2.06 is used;
F.A. Berends, P.H. Daverfeldt and R. Kleiss, Nucl. Phys. **B 253** (1985) 441.

[23] GGG version 2.03 is used;
F.A. Berends and R. Kleiss, Nucl. Phys. **B 186** (1981) 22.

[24] TEEGG version 7.1 is used;
D. Karlen, Nucl. Phys. **B 289** (1987) 23.

[25] GEANT version 3.15 is used;
R. Brun *et al.*, preprint CERN DD/EE/84-1 (1984); revised 1987.

The L3 Collaboration:

P.Achard,[20] O.Adriani,[17] M.Aguilar-Benitez,[25] J.Alcaraz,[25] G.Alemanni,[23] J.Allaby,[18] A.Aloisio,[29] M.G.Alviggi,[29] H.Anderhub,[49] V.P.Andreev,[6,34] F.Anselmo,[8] A.Arefiev,[28] T.Azemoon,[3] T.Aziz,[9] P.Bagnaia,[39] A.Bajo,[25] G.Baksay,[26] L.Baksay,[26] S.V.Baldew,[2] S.Banerjee,[9] Sw.Banerjee,[4] A.Barczyk,[49,47] R.Barillère,[18] P.Bartalini,[23] M.Basile,[8] N.Batalova,[46] R.Battiston,[33] A.Bay,[23] F.Becattini,[17] U.Becker,[13] F.Behner,[49] L.Bellucci,[17] R.Berbeco,[3] J.Berdugo,[25] P.Berges,[13] B.Bertucci,[33] B.L.Betev,[49] M.Biasini,[33] M.Biglietti,[29] A.Biland,[49] J.J.Blaising,[4] S.C.Blyth,[35] G.J.Bobbink,[2] A.Böhm,[1] L.Boldizsar,[12] B.Borgia,[39] S.Bottai,[17] D.Bourilkov,[49] M.Bourquin,[20] S.Braccini,[20] J.G.Branson,[41] F.Brochu,[4] J.D.Burger,[13] W.J.Burger,[33] X.D.Cai,[13] M.Capell,[13] G.Cara Romeo,[8] G.Carlino,[29] A.Cartacci,[17] J.Casaus,[25] F.Cavallari,[39] N.Cavallo,[36] C.Cecchi,[33] M.Cerrada,[25] M.Chamizo,[20] Y.H.Chang,[44] M.Chemarin,[24] A.Chen,[44] G.Chen,[7] G.M.Chen,[7] H.F.Chen,[22] H.S.Chen,[7] G.Chiefari,[29] L.Cifarelli,[40] F.Cindolo,[8] I.Clare,[13] R.Clare,[38] G.Coignet,[4] N.Colino,[25] S.Costantini,[39] B.de la Cruz,[25] S.Cucciarelli,[33] R.de Asmundis,[29] P.Déglon,[20] J.Debreczeni,[12] A.Degré,[4] K.Dehmelt,[26] K.Deiters,[47] D.della Volpe,[29] E.Delmeire,[20] P.Denes,[37] F.DeNotaristefani,[39] A.De Salvo,[49] M.Diemoz,[39] M.Dierckxsens,[2] C.Dionisi,[39] M.Dittmar,[49] A.Doria,[29] M.T.Dova,[10,♯] D.Duchesneau,[4] M.Duda,[1] B.Echenard,[20] A.Eline,[18] A.El Hage,[1] H.El Mamouni,[24] A.Engler,[35] F.J.Eppling,[13] P.Extermann,[20] M.A.Falagan,[25] S.Falciano,[39] A.Favara,[32] J.Fay,[24] O.Fedin,[34] M.Felcini,[49] T.Ferguson,[35] H.Fesefeldt,[1] E.Fiandrini,[33] J.H.Field,[20] F.Filthaut,[31] P.H.Fisher,[13] W.Fisher,[37] I.Fisk,[41] G.Forconi,[13] K.Freudenreich,[49] C.Furetta,[27] Yu.Galaktionov,[28,13] S.N.Ganguli,[9] P.Garcia-Abia,[25] M.Gataullin,[32] S.Gentile,[39] S.Giagu,[39] Z.F.Gong,[22] G.Grenier,[24] O.Grimm,[49] M.W.Gruenewald,[16] M.Guida,[40] V.K.Gupta,[37] A.Gurtu,[9] L.J.Gutay,[46] D.Haas,[5] D.Hatzifotiadou,[8] T.Hebbeker,[1] A.Hervé,[18] J.Hirschfelder,[35] H.Hofer,[49] M.Hohlmann,[26] G.Holzner,[49] S.R.Hou,[44] B.N.Jin,[7] P.Jindal,[14] L.W.Jones,[3] P.de Jong,[2] I.Josa-Mutuberría,[25] M.Kaur,[14] M.N.Kienzle-Focacci,[20] J.K.Kim,[43] J.Kirkby,[18] W.Kittel,[31] A.Klimentov,[13,28] A.C.König,[31] M.Kopal,[46] V.Koutsenko,[13,28] M.Kräber,[49] R.W.Kraemer,[35] A.Krüger,[48] A.Kunin,[13] P.Ladron de Guevara,[25] I.Laktineh,[24] G.Landi,[17] M.Lebeau,[18] A.Lebedev,[13] P.Lebrun,[24] P.Lecomte,[49] P.Lecoq,[18] P.Le Coultre,[49] J.M.Le Goff,[18] R.Leiste,[48] M.Levtchenko,[27] P.Levtchenko,[34] C.Li,[22] S.Likhoded,[48] C.H.Lin,[44] W.T.Lin,[44] F.L.Linde,[2] L.Lista,[29] Z.A.Liu,[7] W.Lohmann,[48] E.Longo,[39] Y.S.Lu,[7] C.Luci,[39] L.Luminari,[39] W.Lustermann,[49] W.G.Ma,[22] L.Malgeri,[18] A.Malinin,[28] C.Maña,[25] J.Mans,[37] J.P.Martin,[24] F.Marzano,[39] K.Mazumdar,[9] R.R.McNeil,[6] S.Mele,[18,29] L.Merola,[29] M.Meschini,[17] W.J.Metzger,[31] A.Mihul,[11] H.Milcent,[18] G.Mirabelli,[39] J.Mnich,[1] G.B.Mohanty,[9] G.S.Muanza,[24] A.J.M.Muijs,[2] B.Musicar,[41] M.Musy,[39] S.Nagy,[15] S.Natale,[20] M.Napolitano,[29] F.Nessi-Tedaldi,[49] H.Newman,[32] A.Nisati,[39] T.Novak,[31] H.Nowak,[48] R.Ofierzynski,[49] G.Organtini,[39] I.Pal,[46] C.Palomares,[25] P.Paolucci,[29] R.Paramatti,[39] G.Passaleva,[17] S.Patricelli,[29] T.Paul,[10] M.Pauluzzi,[33] C.Paus,[13] F.Pauss,[49] M.Pedace,[39] S.Pensotti,[27] D.Perret-Gallix,[4] D.Piccolo,[29] F.Pierella,[8] M.Pioppi,[33] P.A.Piroué,[37] E.Pistolesi,[27] V.Plyaskin,[28] M.Pohl,[20] V.Pojidaev,[17] J.Pothier,[18] D.Prokofiev,[34] G.Rahal-Callot,[49] M.A.Rahaman,[9] P.Raics,[15] N.Raja,[9] R.Ramelli,[49] P.G.Rancoita,[27] R.Ranieri,[17] A.Raspereza,[48] P.Razis,[30] D.Ren,[49] M.Rescigno,[39] S.Reucroft,[10] S.Riemann,[48] K.Riles,[3] B.P.Roe,[3] L.Romero,[25] A.Rosca,[48] C.Rosemann,[1] C.Rosenbleck,[1] S.Rosier-Lees,[4] S.Roth,[1] J.A.Rubio,[18] G.Ruggiero,[17] H.Rykaczewski,[49] A.Sakharov,[49] S.Saremi,[6] S.Sarkar,[39] J.Salicio,[18] E.Sanchez,[25] C.Schäfer,[18] V.Schegelsky,[34] H.Schopper,[21] D.J.Schotanus,[31] C.Sciacca,[29] L.Servoli,[33] S.Shevchenko,[32] N.Shivarov,[42] V.Shoutko,[13] E.Shumilov,[28] A.Shvorob,[32] D.Son,[43] C.Souga,[24] P.Spillantini,[17] M.Steuer,[13] D.P.Stickland,[37] B.Stoyanov,[42] A.Straessner,[20] K.Sudhakar,[9] G.Sultanov,[42] L.Z.Sun,[22] S.Sushkov,[1] H.Suter,[49] J.D.Swain,[10] Z.Szillasi,[26,¶] X.W.Tang,[7] P.Tarjan,[15] L.Tauscher,[5] L.Taylor,[10] B.Tellili,[24] D.Teyssier,[24] C.Timmermans,[31] Samuel C.C.Ting,[13] S.M.Ting,[13] S.C.Tonwar,[9] J.Tóth,[12] C.Tully,[37] K.L.Tung,[7] J.Ulbricht,[49] E.Valente,[39] R.T.Van de Walle,[31] R.Vasquez,[46] V.Veszpremi,[26] G.Vesztergombi,[12] I.Vetlitsky,[28] G.Viertel,[49] S.Villa,[38] M.Vivargent,[4] S.Vlachos,[5] I.Vodopianov,[26] H.Vogel,[35] H.Vogt,[48] I.Vorobiev,[35,28] A.A.Vorobyov,[34] M.Wadhwa,[5] Q.Wang,[31] X.L.Wang,[22] Z.M.Wang,[22] M.Weber,[18] S.Wynhoff,[37] L.Xia,[32] Z.Z.Xu,[22] J.Yamamoto,[3] B.Z.Yang,[22] C.G.Yang,[7] H.J.Yang,[3] M.Yang,[7] S.C.Yeh,[45] An.Zalite,[34] Yu.Zalite,[34] Z.P.Zhang,[22] J.Zhao,[22] G.Y.Zhu,[7] R.Y.Zhu,[32] H.L.Zhuang,[7] A.Zichichi,[8,18,19] B.Zimmermann,[49] M.Zöller.[1]

1 III. Physikalisches Institut, RWTH, D-52056 Aachen, Germany[§]
2 National Institute for High Energy Physics, NIKHEF, and University of Amsterdam, NL-1009 DB Amsterdam, The Netherlands
3 University of Michigan, Ann Arbor, MI 48109, USA
4 Laboratoire d'Annecy-le-Vieux de Physique des Particules, LAPP,IN2P3-CNRS, BP 110, F-74941 Annecy-le-Vieux CEDEX, France
5 Institute of Physics, University of Basel, CH-4056 Basel, Switzerland
6 Louisiana State University, Baton Rouge, LA 70803, USA
7 Institute of High Energy Physics, IHEP, 100039 Beijing, China[△]
8 University of Bologna and INFN-Sezione di Bologna, I-40126 Bologna, Italy
9 Tata Institute of Fundamental Research, Mumbai (Bombay) 400 005, India
10 Northeastern University, Boston, MA 02115, USA
11 Institute of Atomic Physics and University of Bucharest, R-76900 Bucharest, Romania
12 Central Research Institute for Physics of the Hungarian Academy of Sciences, H-1525 Budapest 114, Hungary[‡]
13 Massachusetts Institute of Technology, Cambridge, MA 02139, USA
14 Panjab University, Chandigarh 160 014, India
15 KLTE-ATOMKI, H-4010 Debrecen, Hungary[¶]
16 Department of Experimental Physics, University College Dublin, Belfield, Dublin 4, Ireland
17 INFN Sezione di Firenze and University of Florence, I-50125 Florence, Italy
18 European Laboratory for Particle Physics, CERN, CH-1211 Geneva 23, Switzerland
19 World Laboratory, FBLJA Project, CH-1211 Geneva 23, Switzerland
20 University of Geneva, CH-1211 Geneva 4, Switzerland
21 University of Hamburg, D-22761 Hamburg, Germany
22 Chinese University of Science and Technology, USTC, Hefei, Anhui 230 029, China[△]
23 University of Lausanne, CH-1015 Lausanne, Switzerland
24 Institut de Physique Nucléaire de Lyon, IN2P3-CNRS,Université Claude Bernard, F-69622 Villeurbanne, France
25 Centro de Investigaciones Energéticas, Medioambientales y Tecnológicas, CIEMAT, E-28040 Madrid, Spain[♭]
26 Florida Institute of Technology, Melbourne, FL 32901, USA
27 INFN-Sezione di Milano, I-20133 Milan, Italy
28 Institute of Theoretical and Experimental Physics, ITEP, Moscow, Russia
29 INFN-Sezione di Napoli and University of Naples, I-80125 Naples, Italy
30 Department of Physics, University of Cyprus, Nicosia, Cyprus
31 Radboud University and NIKHEF, NL-6525 ED Nijmegen, The Netherlands
32 California Institute of Technology, Pasadena, CA 91125, USA
33 INFN-Sezione di Perugia and Università Degli Studi di Perugia, I-06100 Perugia, Italy
34 Nuclear Physics Institute, St. Petersburg, Russia
35 Carnegie Mellon University, Pittsburgh, PA 15213, USA
36 INFN-Sezione di Napoli and University of Potenza, I-85100 Potenza, Italy
37 Princeton University, Princeton, NJ 08544, USA
38 University of Californa, Riverside, CA 92521, USA
39 INFN-Sezione di Roma and University of Rome, "La Sapienza", I-00185 Rome, Italy
40 University and INFN, Salerno, I-84100 Salerno, Italy
41 University of California, San Diego, CA 92093, USA
42 Bulgarian Academy of Sciences, Central Lab. of Mechatronics and Instrumentation, BU-1113 Sofia, Bulgaria
43 The Center for High Energy Physics, Kyungpook National University, 702-701 Taegu, Republic of Korea
44 National Central University, Chung-Li, Taiwan, China
45 Department of Physics, National Tsing Hua University, Taiwan, China
46 Purdue University, West Lafayette, IN 47907, USA
47 Paul Scherrer Institut, PSI, CH-5232 Villigen, Switzerland
48 DESY, D-15738 Zeuthen, Germany
49 Eidgenössische Technische Hochschule, ETH Zürich, CH-8093 Zürich, Switzerland
§ Supported by the German Bundesministerium für Bildung, Wissenschaft, Forschung und Technologie.
‡ Supported by the Hungarian OTKA fund under contract numbers T019181, F023259 and T037350.
¶ Also supported by the Hungarian OTKA fund under contract number T026178.
♭ Supported also by the Comisión Interministerial de Ciencia y Tecnología.
♯ Also supported by CONICET and Universidad Nacional de La Plata, CC 67, 1900 La Plata, Argentina.
△ Supported by the National Natural Science Foundation of China.

$\langle\sqrt{s}\rangle$ (GeV)	$\mathcal{L}$(pb^{-1})	N_D	N_{MC}	N_S	N_B
188.6	156.4	11561	11559	11288	271
191.6	29.7	1976	1953	1905	48
195.6	83.7	5677	5673	5539	134
199.5	83.5	5382	5338	5201	137
201.8	39.1	2379	2417	2355	62
205.2	75.9	4259	4165	4063	102
206.7	130.4	7388	7512	7339	173
208.2	8.7	441	484	473	11
198.0	607.4	39063	39101	38163	938

Table 1: Luminosity-averaged centre-of-mass energies, $\langle\sqrt{s}\rangle$, and corresponding integrated luminosities, $\mathcal{L}$, used in the analysis. The $\sqrt{s}$ spread in each point is of the order of 1 GeV. The numbers of observed events, N_D, are given together with the total Monte Carlo expectations, N_{MC}, and their breakdown into signal, N_S, and background, N_B, events. The last row lists the average centre-of-mass energy, the total integrated luminosity and the total numbers of events.

		$\mathrm{d}\sigma/\mathrm{d}\lvert\cos\theta\rvert$ (pb)							
		$\langle\sqrt{s}\rangle = 188.6$ GeV		$\langle\sqrt{s}\rangle = 191.6$ GeV		$\langle\sqrt{s}\rangle = 195.6$ GeV		$\langle\sqrt{s}\rangle = 199.5$ GeV	
$\lvert\cos\theta\rvert$	$\langle\lvert\cos\theta\rvert\rangle$	Meas.	Exp.	Meas.	Exp.	Meas.	Exp.	Meas.	Exp.
$0.00-0.09$	0.052	$12.8\pm 0.9\pm 0.2$	10.4	$9.3\pm 1.9\pm 0.2$	10.1	$8.6\pm 1.0\pm 0.1$	9.6	$10.3\pm 1.1\pm 0.2$	9.2
$0.09-0.18$	0.138	$10.9\pm 0.8\pm 0.1$	11.3	$10.2\pm 2.0\pm 0.2$	11.0	$10.5\pm 1.2\pm 0.1$	10.5	$9.8\pm 1.1\pm 0.1$	10.0
$0.18-0.27$	0.227	$14.0\pm 1.0\pm 0.2$	13.4	$11.5\pm 2.1\pm 0.2$	13.0	$12.0\pm 1.2\pm 0.2$	12.4	$12.2\pm 1.3\pm 0.2$	11.9
$0.27-0.36$	0.317	$16.2\pm 1.0\pm 0.1$	17.1	$14.3\pm 2.4\pm 0.2$	16.6	$18.0\pm 1.5\pm 0.2$	15.9	$14.7\pm 1.4\pm 0.2$	15.2
$0.36-0.45$	0.407	$25.0\pm 1.3\pm 0.2$	23.7	$23.6\pm 3.0\pm 0.3$	22.9	$20.6\pm 1.6\pm 0.2$	21.9	$20.0\pm 1.6\pm 0.2$	21.0
$0.45-0.54$	0.497	$35.0\pm 1.6\pm 0.3$	35.3	$30.9\pm 3.5\pm 0.3$	34.2	$32.4\pm 2.1\pm 0.3$	32.8	$28.0\pm 1.9\pm 0.3$	31.5
$0.54-0.63$	0.588	$57.9\pm 2.0\pm 1.1$	57.7	$61.2\pm 5.0\pm 1.2$	55.9	$51.2\pm 2.6\pm 1.0$	53.6	$49.3\pm 2.6\pm 1.0$	51.5
$0.63-0.72$	0.678	$109.8\pm 3.1\pm 2.6$	105.8	$109.4\pm 7.4\pm 2.9$	102.6	$99.3\pm 4.0\pm 2.5$	98.5	$98.9\pm 4.1\pm 2.5$	94.6
$0.72-0.81$	0.770	$227.1\pm 18.2\pm 10.8$	232.2	$196.4\pm 39.3\pm 16.3$	225.1	$211.2\pm 23.6\pm 14.0$	216.2	$231.3\pm 26.9\pm 16.2$	207.7
$0.81-0.90$	0.862	$735.4\pm 8.4\pm 6.3$	735.9	$720.4\pm 19.8\pm 7.3$	713.5	$690.4\pm 11.2\pm 6.4$	685.1	$670.3\pm 11.1\pm 6.2$	658.4
		$\langle\sqrt{s}\rangle = 201.8$ GeV		$\langle\sqrt{s}\rangle = 205.2$ GeV		$\langle\sqrt{s}\rangle = 206.7$ GeV		$\langle\sqrt{s}\rangle = 208.2$ GeV	
$\lvert\cos\theta\rvert$	$\langle\lvert\cos\theta\rvert\rangle$	Meas.	Exp.	Meas.	Exp.	Meas.	Exp.	Meas.	Exp.
$0.00-0.09$	0.052	$11.0\pm 1.7\pm 0.1$	9.0	$8.7\pm 1.2\pm 0.2$	8.8	$9.0\pm 0.9\pm 0.1$	8.6	$3.9\pm 2.3\pm 0.1$	8.5
$0.09-0.18$	0.138	$11.0\pm 1.7\pm 0.1$	9.8	$12.9\pm 1.4\pm 0.2$	9.6	$8.7\pm 0.9\pm 0.1$	9.4	$10.3\pm 3.7\pm 0.2$	9.2
$0.18-0.27$	0.227	$11.9\pm 1.8\pm 0.2$	11.6	$12.3\pm 1.4\pm 0.2$	11.4	$10.4\pm 0.9\pm 0.2$	11.2	$5.4\pm 2.7\pm 0.1$	10.9
$0.27-0.36$	0.317	$14.8\pm 2.1\pm 0.2$	14.9	$16.1\pm 1.6\pm 0.1$	14.6	$16.8\pm 1.2\pm 0.2$	14.3	$13.4\pm 4.2\pm 0.1$	14.0
$0.36-0.45$	0.407	$21.2\pm 2.5\pm 0.2$	20.6	$20.0\pm 1.8\pm 0.2$	20.2	$23.1\pm 1.4\pm 0.3$	19.8	$23.4\pm 5.7\pm 0.3$	19.4
$0.45-0.54$	0.497	$37.2\pm 3.3\pm 0.4$	30.9	$31.7\pm 2.3\pm 0.4$	30.2	$29.4\pm 1.6\pm 0.4$	29.7	$26.3\pm 6.0\pm 0.3$	29.1
$0.54-0.63$	0.588	$55.5\pm 4.1\pm 1.0$	50.5	$48.0\pm 2.8\pm 0.9$	49.5	$44.5\pm 2.0\pm 0.8$	48.5	$37.6\pm 7.2\pm 0.7$	47.6
$0.63-0.72$	0.678	$91.4\pm 5.7\pm 2.3$	92.7	$93.3\pm 4.3\pm 2.3$	90.9	$90.0\pm 3.2\pm 2.4$	89.2	$84.3\pm 12.0\pm 2.3$	87.5
$0.72-0.81$	0.770	$243.7\pm 39.0\pm 18.7$	203.7	$252.2\pm 29.3\pm 15.5$	199.7	$170.0\pm 17.5\pm 14.5$	195.9	$280.3\pm 88.6\pm 24.0$	192.2
$0.81-0.90$	0.862	$618.3\pm 15.8\pm 6.0$	645.7	$628.9\pm 11.9\pm 5.7$	633.3	$604.4\pm 8.7\pm 6.2$	621.2	$565.3\pm 33.0\pm 5.8$	609.5

Table 2: Measured, Meas., and expected, Exp., folded differential cross sections for the eight average centre-of-mass energies, $\langle\sqrt{s}\rangle$, and the ten $\lvert\cos\theta\rvert$ intervals, with expected average values $\langle\lvert\cos\theta\rvert\rangle$. The first uncertainty is statistical and the second systematic.

$\langle \lvert\cos\theta\rvert \rangle$	$\frac{\mathrm{d}\,\sigma}{\mathrm{d}\,\lvert\cos\theta\rvert}$ (pb)	$\frac{\mathrm{d}\,\sigma^{th}(1)}{\mathrm{d}\,\lvert\cos\theta\rvert}$ (pb)	$\frac{\mathrm{d}\,\sigma^{th}(0)}{\mathrm{d}\,\lvert\cos\theta\rvert}$ (pb)
0.052	$9.93 \pm 0.42 \pm 0.15$	9.7	8.6
0.138	$10.25 \pm 0.43 \pm 0.21$	10.5	9.4
0.227	$11.99 \pm 0.47 \pm 0.14$	12.4	11.0
0.317	$15.95 \pm 0.54 \pm 0.14$	15.8	14.2
0.407	$22.15 \pm 0.64 \pm 0.25$	21.7	19.7
0.497	$31.65 \pm 0.77 \pm 0.17$	32.2	29.5
0.588	$51.15 \pm 0.99 \pm 0.26$	52.3	48.4
0.678	$98.7 \pm 1.5 \pm 1.2$	95.8	89.1
0.770	$211.6 \pm 9.1 \pm 13.9$	210.2	197.0
0.862	$666.9 \pm 4.1 \pm 4.9$	671.1	634.2

Table 3: Combined differential cross sections for the luminosity-averaged centre-of-mass energy $\langle\sqrt{s}\rangle = 198$ GeV, compared with the Standard Model expectations, $\mathrm{d}\,\sigma^{th}(1)/\mathrm{d}\,|\cos\theta|$, and the expectations for the case in which α does not change with Q^2, $\mathrm{d}\,\sigma^{th}(0)/\mathrm{d}\,|\cos\theta|$. The first uncertainties are statistical and the second systematic.

Source of uncertainty	ΔC
Theoretical uncertainty	0.11
Experimental systematic	0.08
F_{rad}	0.05
Bin migration	< 0.01
Total	0.14

Table 4: Sources of systematic uncertainty and their effect, ΔC, on the determination of the C parameter.

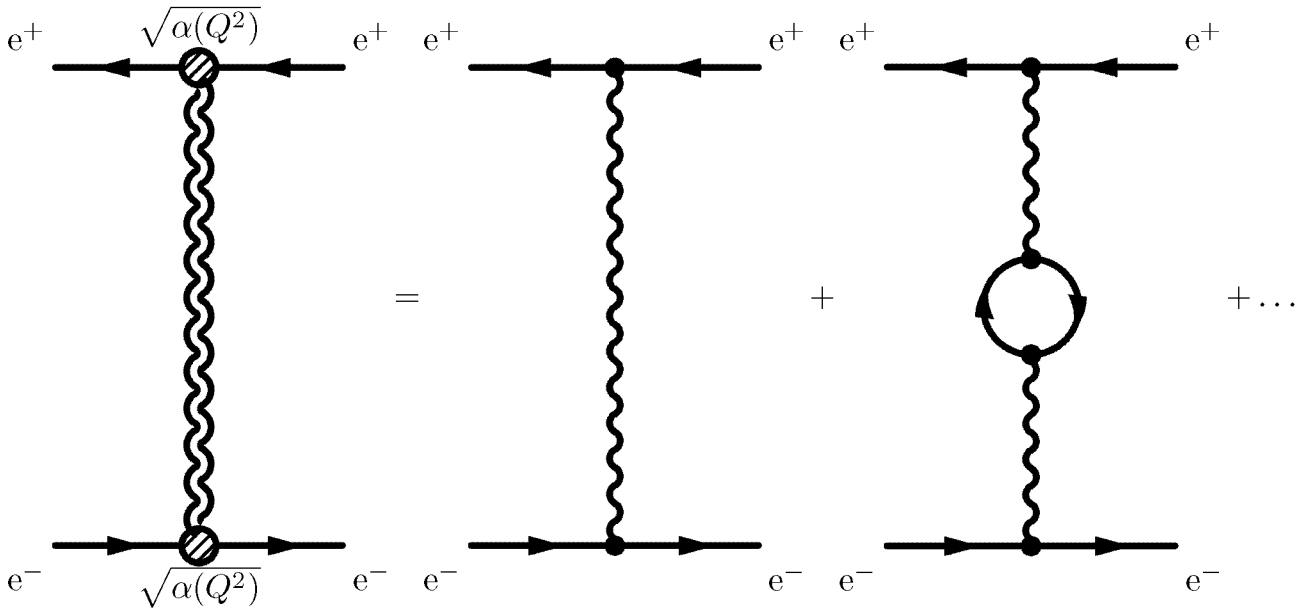

Figure 1: t-channel Feynman diagrams contributing to Bhabha scattering. Diagrams with virtual-fermion vacuum-polarisation insertions generate an electromagnetic coupling $\alpha(Q^2)$. The sum of all diagrams including zero, one, two or more vacuum-polarisation insertions is denoted by the diagram to the left with the double-wavy photon propagator.

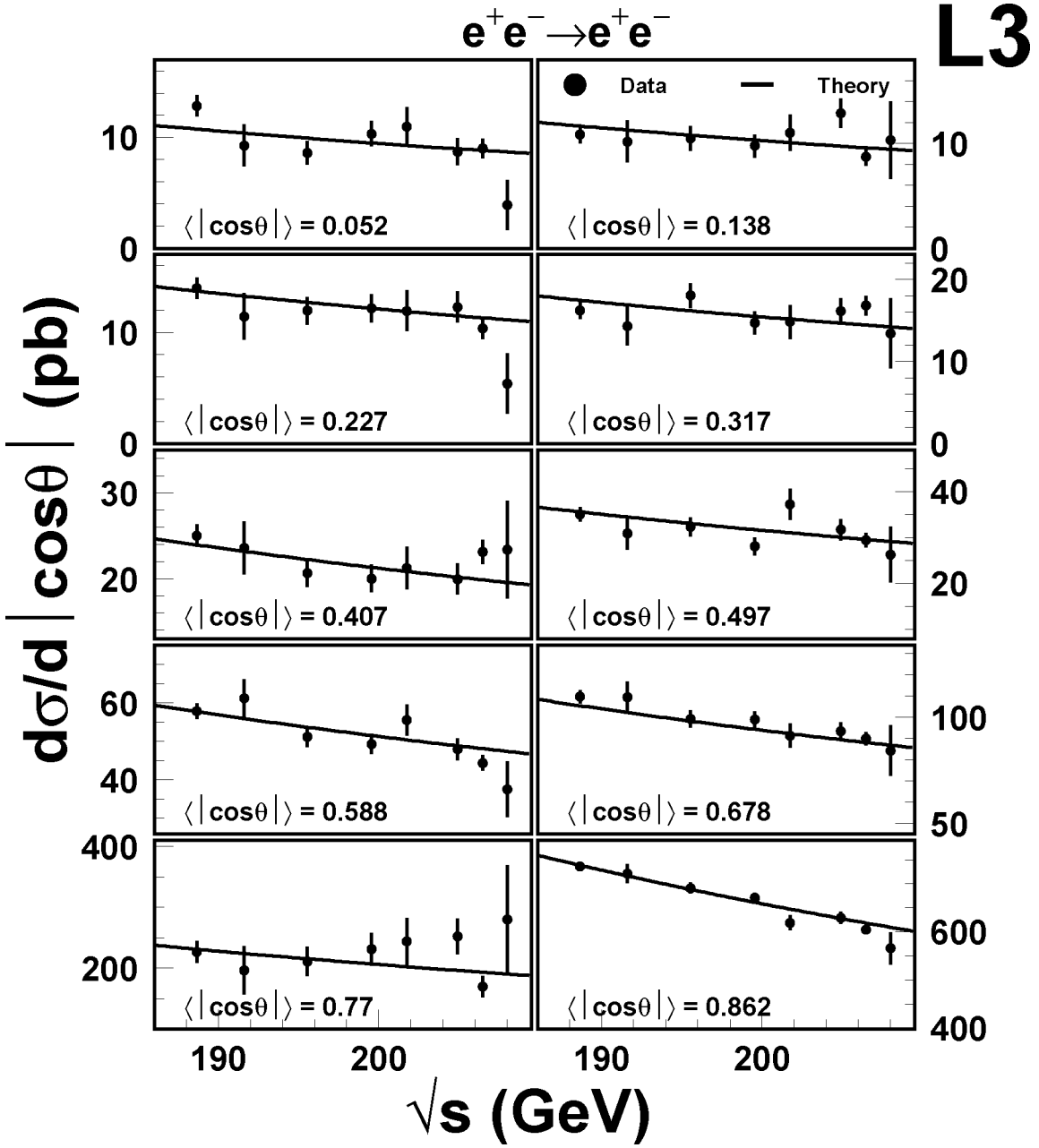

Figure 2: Measured Bhabha differential cross-sections for the ten $|\cos\theta|$ intervals used in the study as a function of the centre-of-mass energy $\sqrt{s}$. The Standard Model predictions are represented by the solid lines.

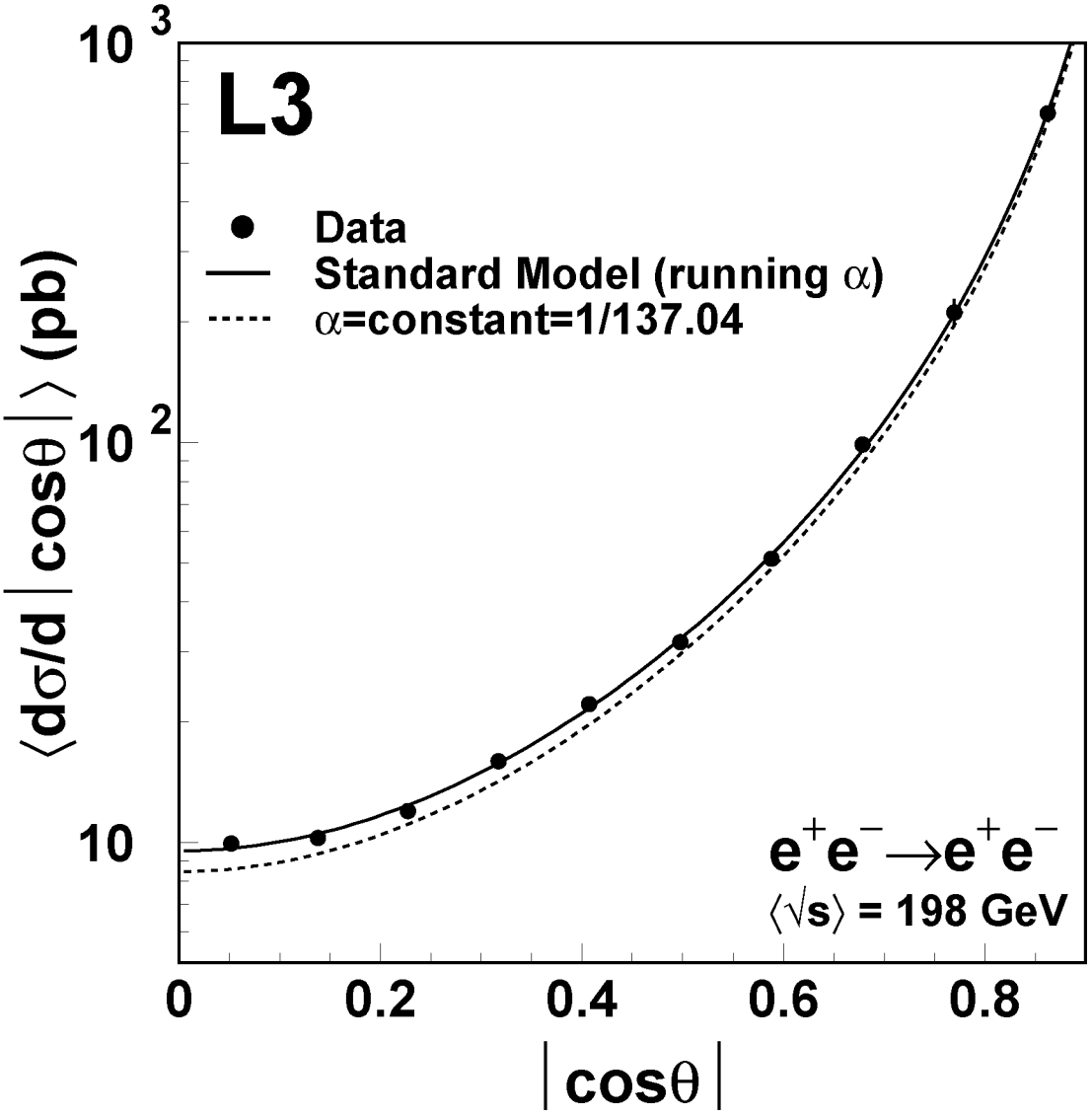

Figure 3: Measured differential cross-section as a function of $|\cos\theta|$. Data at different centre-of-mass energies are combined at the luminosity-averaged centre-of-mass energy $\langle\sqrt{s}\rangle = 198$ GeV. The predictions in case of a running electromagnetic coupling and for a constant value $\alpha = \alpha_0$ are also shown.

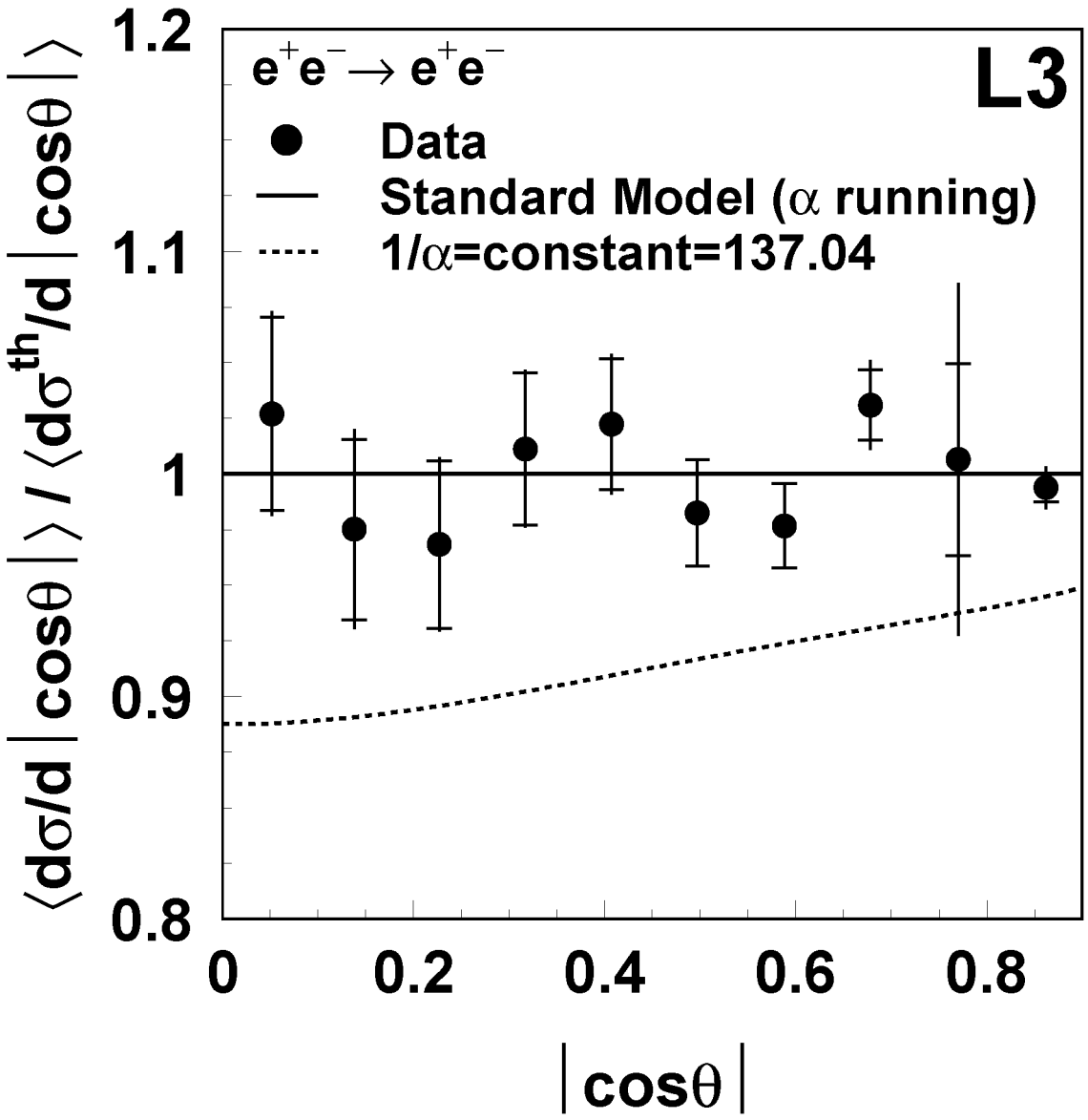

Figure 4: Ratio between the measured Bhabha differential cross section as a function of $|\cos\theta|$ and the Standard Model expectations including a running electromagnetic coupling. Data at different centre-of-mass energies are combined at the luminosity-averaged centre-of-mass energy $\langle\sqrt{s}\rangle = 198$ GeV. The inner error bars represent statistical uncertainties and the full error bars the sum in quadrature of the statistical and systematic uncertainties. The predictions for a constant value of $\alpha = \alpha_0$ are also shown.

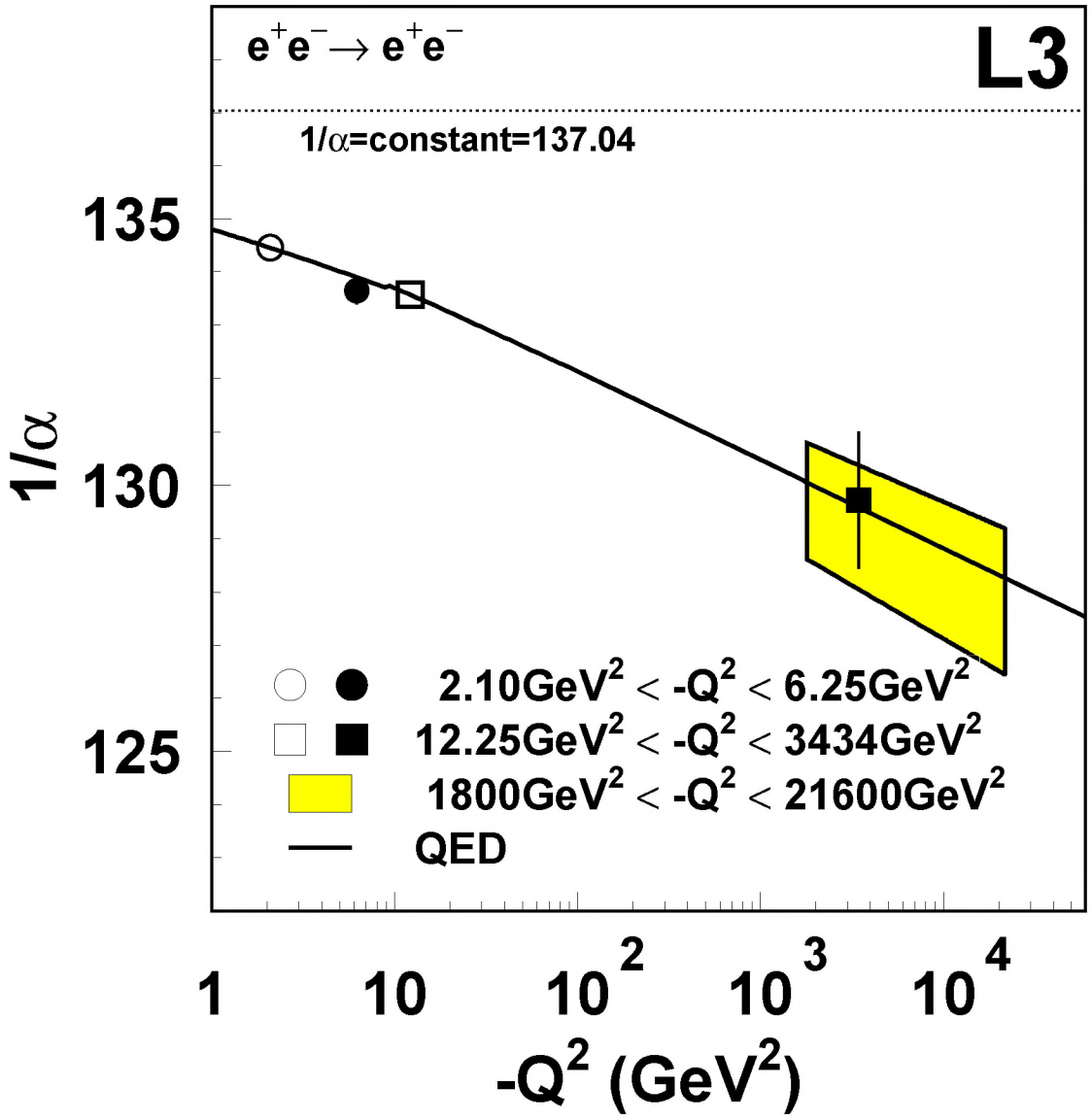

Figure 5: Evolution of the electromagnetic coupling with Q^2 determined from the present measurement of C for 1800 GeV^2 $< -Q^2 <$ 21600 GeV^2, yellow band, and from previous data for Bhabha scattering at 2.10 GeV^2 $< -Q^2 <$ 6.25 GeV^2 and 12.25 GeV^2 $< -Q^2 <$ 3434 GeV^2 [10]. The open symbols indicate the values of Q^2 where $\alpha(Q^2)$ was fixed to the QED predictions [5] in order to infer the values of $\alpha(Q^2)$ shown by the full symbols. These QED predictions are shown by the solid line.

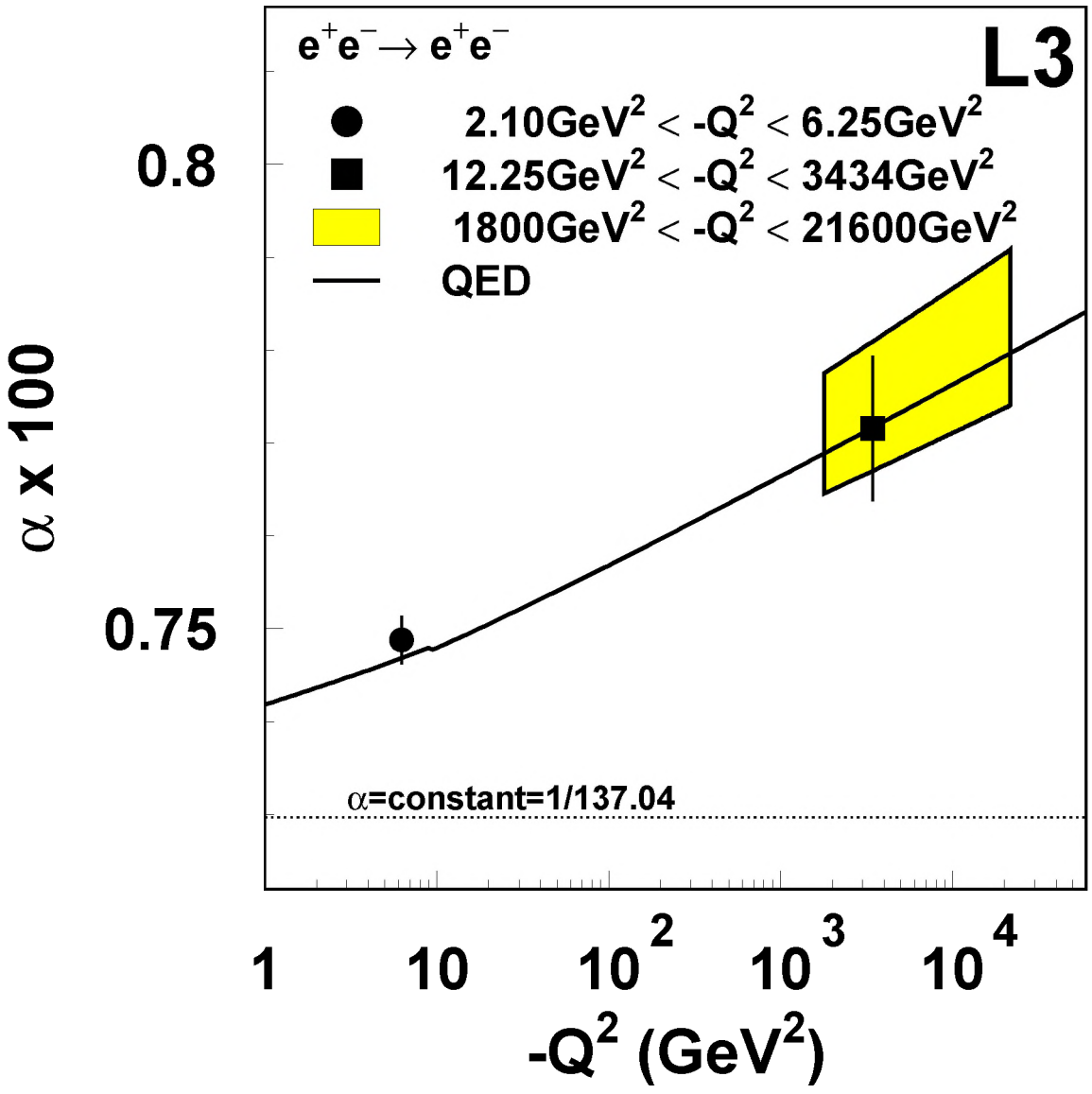

Figure 6: Evolution of the electromagnetic coupling with Q^2 determined from the present measurement of C for 1800 GeV^2 $< -Q^2 <$ 21600 GeV^2, yellow band, and from previous data for Bhabha scattering at 2.10 GeV^2 $< -Q^2 <$ 6.25 GeV^2 and 12.25 GeV^2 $< -Q^2 <$ 3434 GeV^2 [10], full symbols. The solid line represent the QED predictions [5].